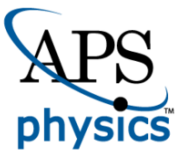

Photodetachment microscopy in time-dependent fields

H. Ambalampitiya and I. I. Fabrikant

Phys. Rev. A **95**, 053414 — Published 24 May 2017

DOI: 10.1103/PhysRevA.95.053414

Photodetachment microscopy in time-dependent fields

H. Ambalampitiya and I. I. Fabrikant

Department of Physics and Astronomy,

University of Nebraska, Lincoln, Nebraska 68588-0111, USA

(Dated: May 4, 2017)

Abstract

Photodetachment of negative ions in combined laser and low-frequency fields is investigated. The time-dependent Green's function method is used for calculation of electron flux at a macroscopic distance away from the photodetachment source, typical for a photodetachment microscopy experiment. In calculating the electron flux, we use the stationary phase method for the time integral, equivalent to the semiclassical approximation, to compute the time dependent wavefunction. The stationary points $t_1^{(i)}$, $i = 1, ..., n$ correspond to time instances of launching of classical trajectories arriving at the detector at a given space-time point $(\mathbf{r}, t)$. The number of trajectories n contributing to the electron flux at any point in the classically allowed space-time domain can be controlled by varying the switching interval of the high frequency laser which initiates the photodetachment process. The divergences inherent in the electron flux in the semiclassical treatment are removed by using the uniform Airy approximation near the caustics.

PACS numbers:

I. INTRODUCTION

Studies of electron photodetachment in external static electric fields demonstrate spatial interference of electrons traveling along different classical trajectories [1–4]. Similar phenomena were predicted for photodetachment in parallel electric and magnetic fields [5–7] and other external fields, particularly due to metallic and dielectric surfaces [8–11]. Experimental observations of spatial interference in static electric fields [12] allow very precise determination of electron affinities [13–15]. These studies have developed in a whole field called "photodetachment microscopy". Similar studies with neutral atoms [16–22] are called "photoionization microscopy". Replacing static electric fields with low-frequency, particular radiofrequency, fields adds new interesting physics [23–26] which was investigated in several recent theoretical studies [27–31]. Yang and Robicheaux [28] showed that time-dependent terahertz fields, in addition to the spatial interference, create also temporal interference. Such studies are important for the general theory of detachment of negative ions and ionization of neutral atoms and molecules by radiation fields. The returning electron trajectories undergo rescattering and this contributes to such interesting phenomena as above-threshold ionization [32], high-order harmonic generation [33, 34] and multielectron nonsequential ionization [35]. Qualitatively the contribution of rescattering to these phenomena is described by the "simple-man" model [36], although the modern computational techniques allow an accurate quantitative description by numerical solution of the time-dependent Schrödinger equation. For the purpose of understanding of more physics, the quasiclassical and semiclassical methods [32, 37], which stand between the simple-man model and exact quantum-mechanical calculations, are becoming quite useful.

There are two types of methods standing between classical and quantum mechanics. Methods of the first type describe the wave function in terms of classical quantities, classical probability density and action [19, 37–39]. The latter is equal to the phase of the wavefunction. If necessary, these quantities can be analytically continued in the complex time plane to describe the motion in classically-forbidden regions [40–43]. However, this extension is not always straightforward. Methods of the second type start with the Schrödinger equation, and then use short-wavelength approximation or stationary phase methods to obtain an approximate wavefunction [42, 44, 45].

In the present paper we use the second approach, but restrict ourselves to classically

allowed region. In this case the electron motion starts above the potential barrier binding the electron in a negative ion. Practically this is achieved by using a high-frequency laser field which detaches electrons and launches classically allowed trajectories in another, static or low-frequency, field. Our approach to description of this process, belonging to the second type, is somewhat different from that of Yang and Robicheaux [28]. We start with the integral form of the Schrödinger equation involving the exact quantum-mechanical propagator for electron motion in a low-frequency field [46]. After calculating the integral in this equation by the stationary phase method, we obtain the electron wavefunction in terms of electron action along classical trajectories. The advantage of this approach is in its generality, since it allows description of classically forbidden trajectories as well with stationary points lying in the complex time plane. It also can be extended to photoionization by inclusion of the Coulomb field in calculation of classical trajectories.

The rest of the paper is organized as follows. In Section II we present the theoretical formulation. In Section III we discuss the behavior of the wavefunction near the caustic. In Section IV we analyze electron trajectories contributing to the flux at the detector. In Section V we present sample results. Sec. VI contains conclusion and outlook. Atomic units are used throughout the paper, unless stated otherwise.

II. THEORETICAL FORMULATION

We start with the time-dependent Schrödinger equation with the Hamiltonian

$$H = H_a + H_s + H_l$$

where H_a is the atomic Hamiltonian containing interaction of the active electron with the atomic residue, and H_s, H_l are electron interactions with the short-wavelength laser field and the long-wavelength (low-frequency) field respectively. The frequency of the laser field should be high enough to allow one-photon detachment of the negative ion, and the frequency of the long-wavelength field can lie between the radiofrequency (rf) and terahertz frequency range. For specific calculations we choose rf fields with frequencies 100 and 200 MHz. We assume that both fields are linearly polarized and parallel, and direct them along the negative z axis. Then in the dipole approximation, using the length gauge, we have

$$H_s = -F_s(t)z, \qquad H_l = -F_l(t)z$$

where $F_s(t)$, $F_l(t)$ are corresponding forces acting on the electron. We assume both fields to be monochromatic, but in order to obtain temporal interference we will switch on the laser field at time t_0 and switch it off at time t_2, so that

$$F_s(t) = \Lambda(t, t_0, t_2)\Phi\cos(\omega_s t + \phi),$$

$$\Lambda(t, t_0, t_2) = f(t - t_0) - f(t - t_2)$$

where Φ is the field amplitude, and ϕ is a phase which does not influence the final result for the electron current. The function $f(t)$ is growing from 0 at $t = -\infty$ to 1 at $t = \infty$ with the switching interval t_s small compared to $t_2 - t_0$. The exact shape of $f(t)$ is not important, as long as

$$2\pi/\omega_s \ll t_s \ll t_2 - t_0. \tag{1}$$

For example, the choice $t_s = 0$, or $f(t) = \eta(t)$, where $\eta(t)$ is the step (Heaviside) function would not satisfy the first condition. Yang and Robicheaux [28] choose $f(t) = [\tanh(t/t_s) + 1]/2$.

For the low-frequency field we have

$$F_l(t) = F_0\cos\omega t$$

and there is no need to limit its duration as long as the duration of the laser pulse is limited. If t_s is sufficiently small, the effective time instant for switching on the laser field is t_0, and the effective time instant for turning off the laser field is t_2. Therefore, by varying t_0 and the time interval $t_2 - t_0$ we can control the initial phase of the low-frequency field and the number of cycles of the low-frequency field which affect the detachment process.

The Schrödinger equation can be written in the following integral form

$$\psi(\mathbf{r}, t) = \int_{-\infty}^{t} dt' \int d\mathbf{r}' G(\mathbf{r}, t, \mathbf{r}', t') H_s(\mathbf{r}', t')\psi(\mathbf{r}', t') \tag{2}$$

where $G(\mathbf{r}, t, \mathbf{r}', t')$ is the electron propagator incorporating the atomic and the low-frequency field, but not the laser field. We then make two approximations typical in these problems [40, 42]. First, we neglect the influence of the atomic field on the propagator. This is equivalent to the neglect of the rescattering effects which are very weak for short-range potentials describing electron interaction with atomic residue in the photodetachment problem [47, 48]. In photoionization problem the Coulomb field of the ion residue should be included. Second,

we neglect the influence of both laser and low-frequency fields on the wave function in the right-hand side of Eq. (2), i.e. we assume

$$\psi(\mathbf{r},t) \approx e^{-iE_b t}\psi_0(\mathbf{r})$$

where E_b is the energy of the initial bound state, and $\psi_0(\mathbf{r})$ is the corresponding bound-state wavefunction. This is justified for weak fields considered in the present paper [42].

For treating the absorption process the interaction Hamiltonian H_s can be replaced by the positive-frequency part

$$H_s = \frac{1}{2}\Lambda(t,t_0,t_2)\Phi z \exp[-i(\omega_s t+\phi)]. \tag{3}$$

Since the laser field is, strictly speaking, not monochromatic, this can raise a question about possible contribution of the negative-frequency part. However, Eq. (3) is valid as long as conditions (1) are satisfied. The integral equation turns now to the following integral representation for $\psi(\mathbf{r},t)$

$$\psi(\mathbf{r},t) = \frac{\Phi e^{-i\phi}}{2}u(\mathbf{r},t)$$

$$u(\mathbf{r},t) = \int_{-\infty}^{t} dt'\Lambda(t',t_0,t_2)e^{-iEt'}\int d\mathbf{r}' G(\mathbf{r},t,\mathbf{r}',t')z'\psi_0(\mathbf{r}') \tag{4}$$

where $E = E_b + \omega$ is the electron energy after detachment. We assume it to be positive.

The quantity of physical interest is the ratio of electron current density at the space-time point $(\mathbf{r},t)$ to the photon current density in the laser field. It does not depend on Φ and ϕ and is given by [4]

$$\frac{j_{el}}{j_{ph}} = \frac{2\pi\omega_s}{c}\mathrm{Im}\left(u^*(\mathbf{r},t)\frac{\partial u(\mathbf{r},t)}{\partial z}\right) \tag{5}$$

where c is the speed of light.

The exact propagator for linearly polarized field is well known, and can be written as [46]

$$G(\mathbf{r},t,\mathbf{r}',t') = -i\eta(t-t')[2\pi i(t-t')]^{-3/2}\exp[iR(\mathbf{r},t,\mathbf{r}',t')] \tag{6}$$

where $R(\mathbf{r},t,\mathbf{r}',t')$ is the principal Hamiltonian function (or action) along the trajectory joining space-time points $(\mathbf{r}',t')$ and $(\mathbf{r},t)$. We denote it by R to distinguish it from the abbreviated action $S_E(\mathbf{r},\mathbf{r}')$ used usually in the problems of electron motion in a static field.

To simplify Eq. (4), we note that the integrand in the right-hand side contains a rapidly oscillating function, and for its calculation we can use the stationary phase method. The equation for the stationary point in t' is

$$\frac{\partial R(\mathbf{r},t,\mathbf{r}',t')}{\partial t'} - E = 0. \tag{7}$$

Using the known relation from the classical mechanics, we obtain

$$H(\mathbf{r}, t, \mathbf{r}', t') = E \tag{8}$$

where H is the classical Hamiltonian of the electron in the low-frequency field expressed as a function of the space-time points $(\mathbf{r}', t')$ and $(\mathbf{r}, t)$. The explicit expressions for R and H can be found using the classical equations of motion. Since both high and low frequency fields are linearly polarized along the z axis, we can use the cylindrical symmetry of the system to constrain the outgoing electron trajectories to a plane with a constant azimuthal angle $\varphi = 0$. With these conditions, classical equations of motion of the electrons in the low-frequency field are as follows,

$$\begin{aligned} x(t) &= \dot{x}'(t - t') + x' \\ z(t) &= -\frac{F_0}{m\omega^2}(\cos\omega t - \cos\omega t') + (t - t')(\dot{z}' - \frac{F_0}{m\omega}\sin\omega t') + z' \end{aligned} \tag{9}$$

where the primed quantities represent the initial space-time coordinates and components of velocity. Now, using Eq.(9), we can write down the analytical expressions for $R(\mathbf{r}, t, \mathbf{r}', t')$ and $H(\mathbf{r}, t, \mathbf{r}', t')$ (see, for example, [49]):

$$\begin{aligned} R(\mathbf{r}, t, \mathbf{r}', t') = \frac{m}{2(t - t')}[(x - x')^2 + (z - z')^2] \\ + F_0\Big(\frac{1}{\omega^2}\frac{(z - z')}{(t - t')}(\cos\omega t - \cos\omega t') + \frac{1}{\omega}(z\sin\omega t - z'\sin\omega t')\Big) \\ + F_0^2\Big(\frac{1}{2m\omega^4}\frac{(\cos\omega t - \cos\omega t')^2}{(t - t')} + \frac{1}{8m\omega^3}(\sin 2\omega t - \sin 2\omega t') - \frac{(t - t')}{4m\omega^2}\Big) \end{aligned} \tag{10}$$

$$\begin{aligned} H(\mathbf{r}, t, \mathbf{r}', t') = \frac{m}{2}\Big(\frac{x - x'}{t - t'}\Big)^2 \\ + \frac{m}{2}\Big(\frac{z - z' + \frac{F_0}{m\omega^2}[\cos\omega t - \cos\omega t']}{t - t'} + \frac{F_0}{m\omega}\sin\omega t'\Big)^2 - F_0 z'\cos\omega t' \end{aligned} \tag{11}$$

We emphasize that R, H, and the preexponential factor in Eq. (6) can be written in analytical forms because we are dealing with photodetachment. For photoionization problem the Coulomb field should be included. This can be done by numerical calculation of classical trajectories in the superposition of the low-frequency field and the Coulomb field.

The integral in the right-hand side of Eq.(4) can be calculated now by the stationary phase method

$$g(\mathbf{r},t,\mathbf{r}') \equiv \int_{-\infty}^{t} dt' \Lambda(t',t_0,t_2) e^{-iEt'} G(\mathbf{r},t,\mathbf{r}',t') =$$
$$-\frac{e^{-i\pi/4}}{2\pi} \sum_{t_1} \frac{\Lambda(t_1,t_0,t_2)}{(t-t_1)^{3/2}} \left| \frac{\partial^2 R}{\partial (t')^2} \right|_{t'=t_1}^{-1/2} \exp\{i[R(\mathbf{r},t,\mathbf{r}',t_1) - Et_1 \pm \pi/4]\} \qquad (12)$$

where the sum is over all solutions t_1 of Eq. (8), and the sign in the exponent is determined by the sign of $\partial^2 R/\partial (t')^2$. If the switching time t_s is short enough, the solutions of Eq.(8) should be chosen from the interval $t_0 < t' < t$, if $t < t_2$, and from the interval $t_0 < t' < t_2$, if $t > t_2$. On the other hand, t_s should not be too short. If, for example, it is chosen to be 0, then the boundaries t_0 and t_2 can contribute to the integral as well, in addition to the stationary points. We therefore require that t_s satisfies conditions (1). Under these conditions, the switching function $\Lambda(t_1,t_0,t_2)$ allows us, by varying t_0 and t_2, select the number of stationary points t_1 which physically correspond to the times of launching of trajectories. In this way we control the number of classical trajectories contributing to the electron current at the space-time point $(\mathbf{r},t)$.

For calculation of the spatial integral in Eq. (4) we note that whereas the coordinates $\mathbf{r}$ are allowed to reach macroscopic values, the coordinates $\mathbf{r}'$ are limited by the spatial extent of the wave function $\psi_0(\mathbf{r}')$. Following [4], we therefore expand $R(\mathbf{r},t,\mathbf{r}',t_1) - Et_1$ in powers of $\mathbf{r}'$. Note also that because of Eq. (8) t_1 is an implicit function of $\mathbf{r}$, $\mathbf{r}'$ and t. Therefore

$$R[\mathbf{r},t,\mathbf{r}',t_1(\mathbf{r},\mathbf{r}',t)] - Et_1(\mathbf{r},\mathbf{r}',t) = R[\mathbf{r},t,\mathbf{0},t_1(\mathbf{r},0,t)] + \left.\frac{\partial R}{\partial \mathbf{r}'}\right|_{\mathbf{r}'=0} \cdot \mathbf{r}'$$
$$+ \left.\frac{\partial R}{\partial t_1}\frac{\partial t_1}{\partial \mathbf{r}'}\right|_{\mathbf{r}'=\mathbf{0}} \cdot \mathbf{r}' - Et_1(\mathbf{r},\mathbf{0},t) - E \left.\frac{\partial t_1}{\partial \mathbf{r}'}\right|_{\mathbf{r}'=\mathbf{0}} \cdot \mathbf{r}'. \qquad (13)$$

According to Eq. (7), terms with $\partial t_1/\partial \mathbf{r}'$ cancel each other, and we obtain

$$R(\mathbf{r},t,\mathbf{r}',t_1) - Et_1 = S_E(\mathbf{r},t) - \mathbf{p}'(\mathbf{r},t,\mathbf{0},t_1) \cdot \mathbf{r}'$$

where

$$S_E(\mathbf{r},t) = R[\mathbf{r},t,\mathbf{0},t_1(\mathbf{r},\mathbf{0},t)] - Et_1(\mathbf{r},\mathbf{0},t) \qquad (14)$$
$$\mathbf{p}'(\mathbf{r},t,\mathbf{0},t_1) = -\left.\frac{\partial R}{\partial \mathbf{r}'}\right|_{\mathbf{r}'=\mathbf{0}}$$

is the momentum of electron launched at the origin at time t_1 and arriving at the space-time point $(\mathbf{r},t)$.

The function $S_E(\mathbf{r},t)$ which we will call a modified action, reminds somewhat the abbreviated action used in stationary problems [1, 4]. However, there are two important differences: first, the energy E is not a conserved quantity. Second, the sign of the second term in Eq. (14) is negative since it contains the initial time t_1 rather than final time t.

The spatial integration is reduced now to calculation of the well-known matrix element

$$M(\mathbf{p}') = \int e^{-i\mathbf{p}'\cdot\mathbf{r}'} z' \psi_0(\mathbf{r}') d\mathbf{r}'.$$

For photodetachment of H^- we can use the zero-range-potential approximation with readjusted normalization constant [50]. Then

$$\psi_0(\mathbf{r}) = B\frac{e^{-r/a}}{r}$$

where $a = (-2E_b)^{-1/2}$, and

$$M(\mathbf{p}') = \frac{8\pi i B p'}{[a^{-2} + (p')^2]^2} \cos\chi'$$

where χ' is the angle between $\mathbf{p}'$ and the z axis.

Finally

$$u(\mathbf{r},t) = -\frac{e^{-i\pi/4}}{2\pi} \sum_{t_1} M(\mathbf{p}')\Lambda(t_1,t_0,t_2)(t-t_1)^{-3/2} \left|\frac{\partial^2 R}{\partial (t')^2}\right|^{-1/2}_{t=t_1} \exp\{i[S(\mathbf{r},t) \pm \pi/4]\}. \quad (15)$$

This should be substituted in Eq. (5) for calculation of the ratio of the current densities.

III. WAVEFUNCTION NEAR CAUSTIC

Before we move on to the description of the wavefunction near the caustic surface, we first briefly investigate the formation of caustics due to the photodetached electron trajectories in time-dependent fields. As the final time t evolves at an arbitrary point on the detector, new pairs of trajectories emerge from the complex space-time domain. In Fig.1, we show how the trajectories start to appear in pairs at the center of the detector. Here , we have drawn $\frac{\partial S}{\partial t'}$ as a function of t' with $t' \in [t_0, t]$ for some fixed final times. According to Fig. 1, when the final time t gradually increases, the curve $\frac{\partial S}{\partial t'}$ passes through a special point

in initial time, denoted by $t' = t_c(\mathbf{r}', \mathbf{r}, t)$. At this point, the following two conditions are simultaneously satisfied.

$$\left.\frac{\partial R}{\partial t'}\right|_{t'=t_c} = E$$
$$\left.\frac{\partial^2 R}{\partial (t')^2}\right|_{t'=t_c} = 0 \tag{16}$$

We say that the two equations (16) define a caustic surface which is the boundary for classically allowed trajectories in space-time domain. In other words, if we launch an ensemble of trajectories from the source at $\mathbf{r}' = \mathbf{0}$ at a fixed initial time t', the set of points, $(\mathbf{r}, t)$, in the real space-time domain satisfying the above conditions are said to lie on the caustic surface, which in general depends on the initial time t'. In Fig.2, we show electron trajectories and the projection of the caustic surface on the $x - z$ plane for three different initial times. Note that trajectories do not cross the caustic surface in the 3-dimensional (x, z, t) space. Apparent crossing points in the $x - z$ plane observed in Fig. 2 do not represent actual crossings.

In the case of a static field, the caustic surface can be obtained from similar equations

$$\frac{\partial R}{\partial \tau} = -E, \quad \frac{\partial^2 R}{\partial \tau^2} = 0$$

where $\tau = t - t'$. These two equations can readily be simplified to obtain an equation for the caustic surface in configuration space which is independent of the launching time.

$$\left(1 + \frac{zF}{E}\right)\left(1 + \frac{z'F}{E}\right) - \frac{F^2}{4E^2}(x - x')^2 = 0.$$

Fig.3 shows the caustic surface as an envelope of electron trajectories for a static field.

On the caustic Eq. (12) is not valid. The integral can be evaluated by expanding the action in powers of $t - t_c$ where $t_c(\mathbf{r}, \mathbf{r}', t)$ is the solution of the equation (16). Introduce again the modified action

$$S(\mathbf{r}, t, \mathbf{r}', t') = R(\mathbf{r}, t, \mathbf{r}', t') - Et'.$$

Then in the vicinity of the caustic

$$S(\mathbf{r}, t, \mathbf{r}', t') = b(\mathbf{r}, \mathbf{r}', t)(t' - t_c) + a(\mathbf{r}, \mathbf{r}', t)(t' - t_c)^3$$

where

$$b(\mathbf{r}, \mathbf{r}', t) = \left.\frac{\partial S}{\partial t'}\right|_{t'=t_c}, \qquad a(\mathbf{r}, \mathbf{r}', t) = \frac{1}{6}\left.\frac{\partial^3 S}{\partial (t')^3}\right|_{t'=t_c}.$$

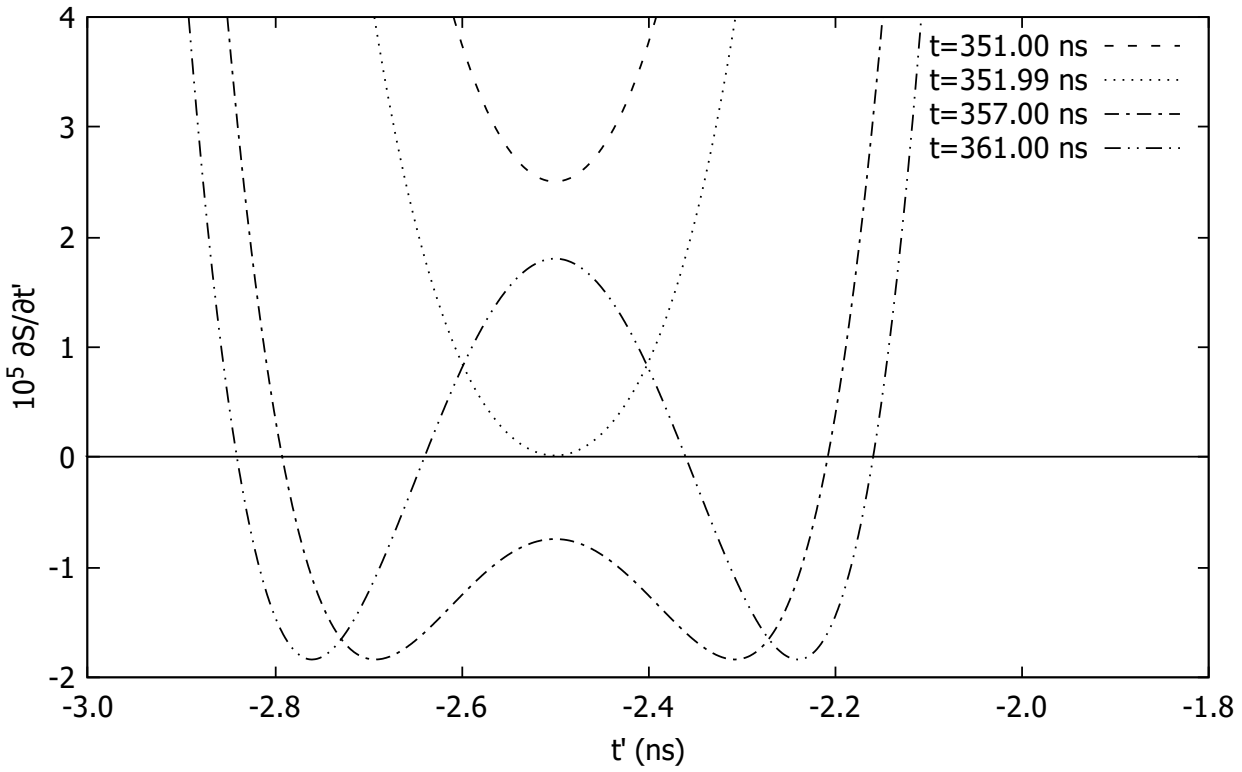

FIG. 1: Graphical solution of the equation $\partial S/\partial t' = 0$ for t' at different detection times t. For t=351.0 ns no real roots exist. This means, there are no real trajectories arriving at the center of the detector. For t=357.00 ns there are two roots corresponding to two electron trajectories arriving at the center of the detector at the same time. Amplitude and the frequency of the field are 50 V/cm and 100 MHz respectively. The detector is 0.5 m away from the source.

Assuming now that $t \gg t_c$ and using the integral representation of the Airy function, we obtain

$$g(\mathbf{r}, t, \mathbf{r}') = -\frac{\exp[i(S(\mathbf{r}, t, \mathbf{r}', t_c))]}{(2\pi i)^{1/2}(t - t_c)^{3/2}[3a(\mathbf{r}, \mathbf{r}', t)]^{1/3}} \mathrm{Ai}\left[\frac{b(\mathbf{r}, \mathbf{r}', t)}{(3a(\mathbf{r}, \mathbf{r}', t))^{1/3}}\right].$$

For calculation of the spatial integral in Eq. (4) we perform the expansion similar to (13). Using

$$\left.\frac{\partial S(\mathbf{r}, t, 0, t')}{\partial t'}\right|_{t'=t_c} = H(\mathbf{r}, t, 0, t_c) - E, \qquad \left.\frac{\partial S(\mathbf{r}, t, \mathbf{r}', t')}{\partial \mathbf{r}'}\right|_{\mathbf{r}'=0} = -\mathbf{p}'(\mathbf{r}, t, 0, t_c),$$

we obtain

$$S(\mathbf{r}, t, \mathbf{r}', t_c) = S(\mathbf{r}, t, 0, t_c) - \mathbf{p}'(\mathbf{r}, t, 0, t_c) \cdot \mathbf{r}' + [H(\mathbf{r}, t, 0, t_c) - E] \left.\frac{\partial t_c}{\partial \mathbf{r}'}\right|_{\mathbf{r}'=0} \cdot \mathbf{r}'.$$

Finally

$$u(\mathbf{r}, t) = -\frac{\exp[i(S(\mathbf{r}, t, 0, t_c))]}{(2\pi i)^{1/2}(t - t_c)^{3/2}[3a(\mathbf{r}, 0, t)]^{1/3}} \mathrm{Ai}\left[\frac{b(\mathbf{r}, 0, t)}{(3a(\mathbf{r}, 0, t))^{1/3}}\right] M(\mathbf{p}_c)$$

where

$$\mathbf{p}_c = \mathbf{p}' - [H(\mathbf{r}, t, 0, t_c) - E] \left.\frac{\partial t_c}{\partial \mathbf{r}'}\right|_{\mathbf{r}'=0}.$$

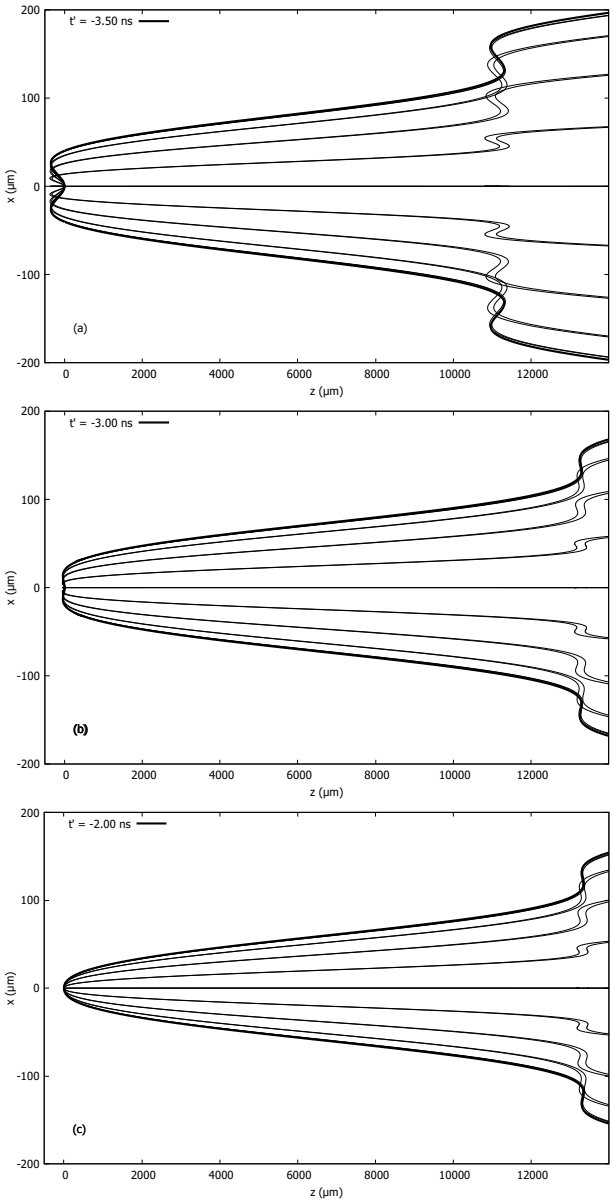

FIG. 2: Electron trajectories (thin lines) and projections of the caustic surfaces on the $x - z$ plane (thick lines). Panels (a),(b) and (c) show the variation of the caustic surface for different initial times.

IV. TRAJECTORY ANALYSIS

In all calculations we assume that electrons reach a planar detector, oriented perpendicular to the z axis, at a distance 0.5 m from the negative ion which is placed at the origin of our coordinate system. The amplitude and the oscillation frequency of the low-frequency field are 50 V/cm and 100 MHz respectively. The electron starts its motion in the classically allowed region with an initial kinetic energy E=0.5 meV after the photodetachment process. It is important to note here that this energy E is not a constant along

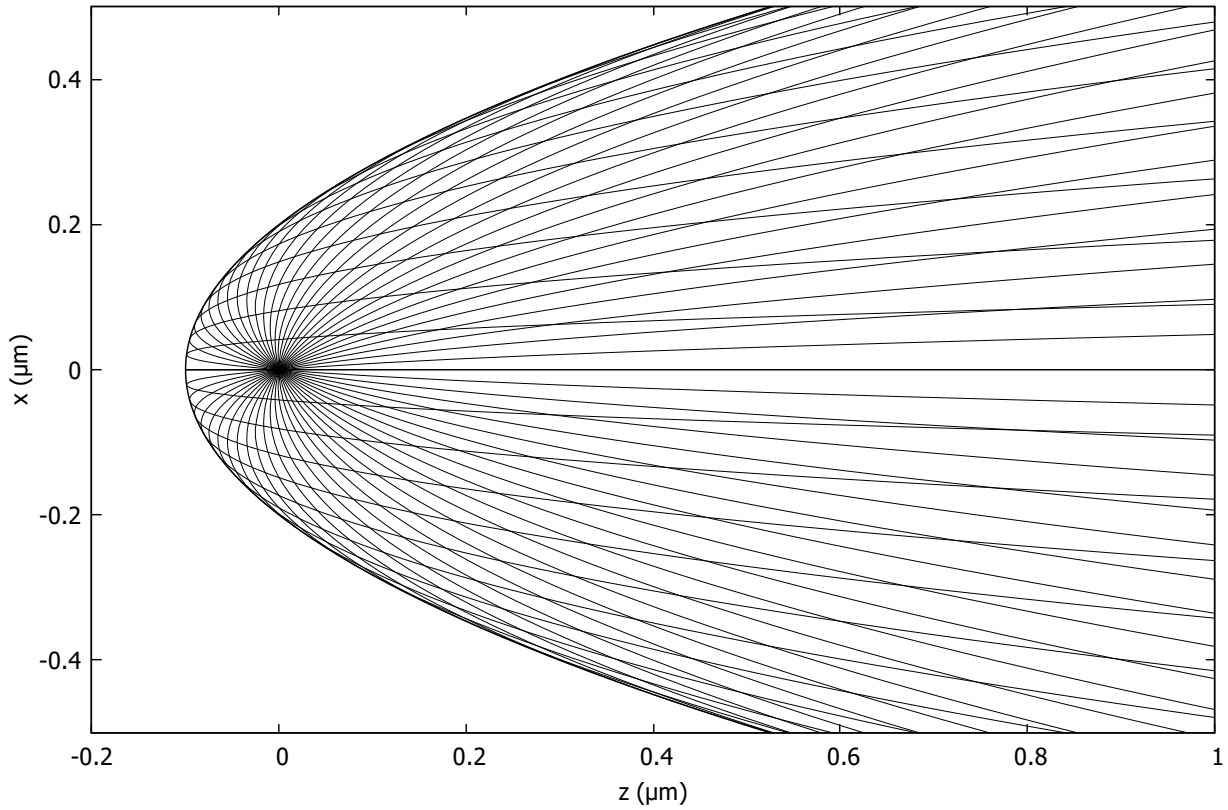

FIG. 3: Electron trajectories (thin lines) and the caustic surface (thick solid line) for the case of a static field. F=50 V/cm, E=0.5 meV

the electron's trajectory. The incident photon energy corresponding to electron's initial kinetic energy is $\omega_s = E - E_b = 0.7556026$ eV where $E_b = -0.7551026$ eV is the electron energy in H^-. The stationary phase condition (8) generates the launching time t' for given launching position $\mathbf{r}'$, final position $\mathbf{r}$ and detection time t, and allows us to find the corresponding trajectory. We choose two suitable laser on-off intervals for the high-frequency field, $I_1 = [t_0, t_2] = [-10\text{ns}, 0\text{ns}]$ and $I_2 = [t_0, t_2] = [-10\text{ns}, 10\text{ns}]$. The durations of the laser intervals are multiples of the period of the low-frequency field. For the switching function (envelope function), $\Lambda(t, t_0, t_2)$, we consider the following two trial functions where the first one is the same as that of Yang and Robicheaux [28].

$$\Lambda_1(t, t_0, t_2) = \frac{1}{2}\Big[\tanh\Big(\frac{t - t_0}{t_s}\Big) - \tanh\Big(\frac{t - t_2}{t_s}\Big)\Big] \tag{17}$$

$$\Lambda_2(t, t_0, t_2) = \frac{1}{\pi}\Big[\tan^{-1}\Big(\frac{t - t_0}{t_s}\Big) - \tan^{-1}\Big(\frac{t - t_2}{t_s}\Big)\Big] \tag{18}$$

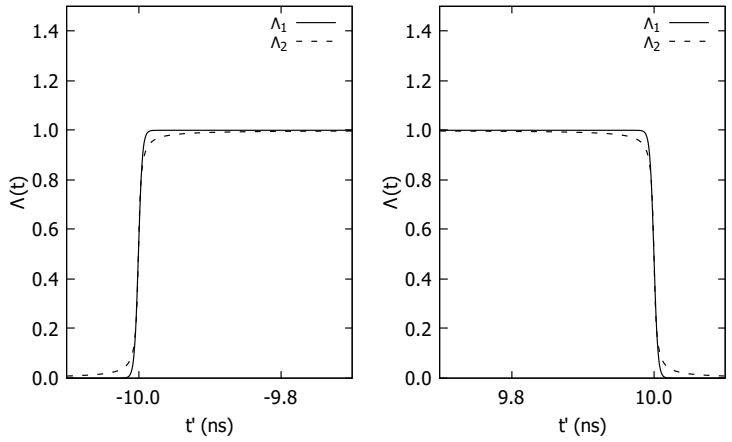

FIG. 4: Profile of $\Lambda(t, t_0, t_2)$ for the laser interval I_2

where the switching interval is t_s=500×2π/ω_s. Fig.4 shows the shapes of the switching functions $\Lambda_1(t, t_0, t_2)$ and $\Lambda_2(t, t_0, t_2)$ for the laser on-off interval I_2. Although the first type of switching occurs faster, both functions satisfy conditions (1), and the results do not depend on the specific choice of Λ.

As the duration of the laser interval increases, the number of electron trajectories arriving at the detector at the same time t increases as well. In Fig. 5 we show the solutions t' for each final time t for the two intervals I_1 and I_2. In Fig.5 (a), for large t, there are 8 trajectories which can be separated into two groups G_1 and G_2 arriving at the detector at the same final time t. The difference between the modified actions, $\Delta S = S(\mathbf{r}, t'^{(1)}) - S(\mathbf{r}, t'^{(2)})$, where S is given by Eq. (14), corresponding to trajectories of groups G_1 and G_2 with starting times $t'^{(1)}$ and $t'^{(2)}$, is large and the interference pattern they produce is rapidly oscillating. This is expected because the earlier trajectories in group G_1 spend more time in the low frequency field than the trajectories in group G_2. In Fig.5 (b), we draw the initial times for electron trajectories corresponding to the laser interval I_1. Now for large t, we can observe a maximum of 4 electron trajectories arriving at the detector center. Here the labels C_1 and C_2 mark the points where the conditions in (16) are simultaneously satisfied. The semiclassical flux is diverging at temporal or spatial caustics, and we will see these divergences as special features in the temporal or spatial interference profiles in the next section. Well beyond the two caustics in Fig.5(b), ΔS between A_1 trajectories and A_2 trajectories also grows rapidly due to the same reason as in Fig.5(a). Therefore, the 4 trajectory interference structure

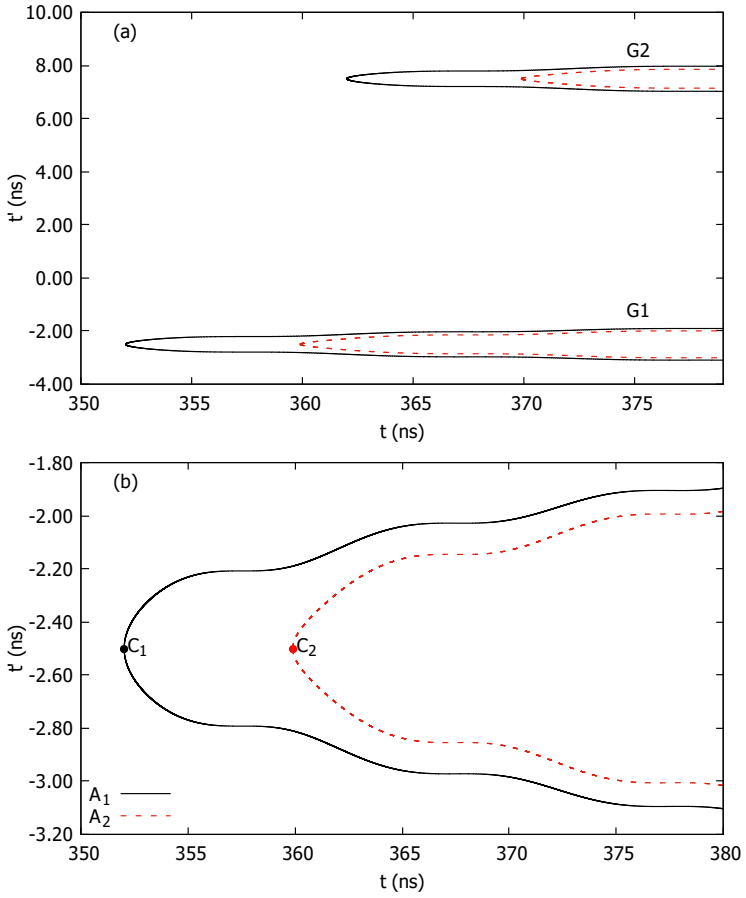

FIG. 5: Relation between the detection time t and the launching time t'. Panel (a): The switching interval is I_2. Maximum of 8 trajectories grouped as G_1 and G_2 are possible. Panel (b): Switching interval I_1. Maximum of 4 trajectories grouped as A_1 and A_2 are possible. C_1 and C_2 indicate the points of the caustic condition (16).

exhibits rapid oscillations. The two trajectories in either of the groups A_1 or A_2 have a very small initial time separation ($\Delta t'$) and thus a small ΔS producing less rapid oscillations.

V. TEMPORAL AND SPATIAL INTERFERENCE

Taking the switching interval I_1, we now compute the ratio given by Eq.(5) with $u(\mathbf{r}, t)$ calculated via Eq. (15). In calculation of the numerical derivative $\partial u(\mathbf{r}, t)/\partial z$, we have to make sure that the increment dz is small enough so that at the new location,$z + dz$, we get the same number of trajectories arriving at time t.

In Fig.6 and Fig.7, we show the electron flux calculated using semiclassical and uniform Airy approximations. In Fig.8, we also show the electron flux when the rf frequency is

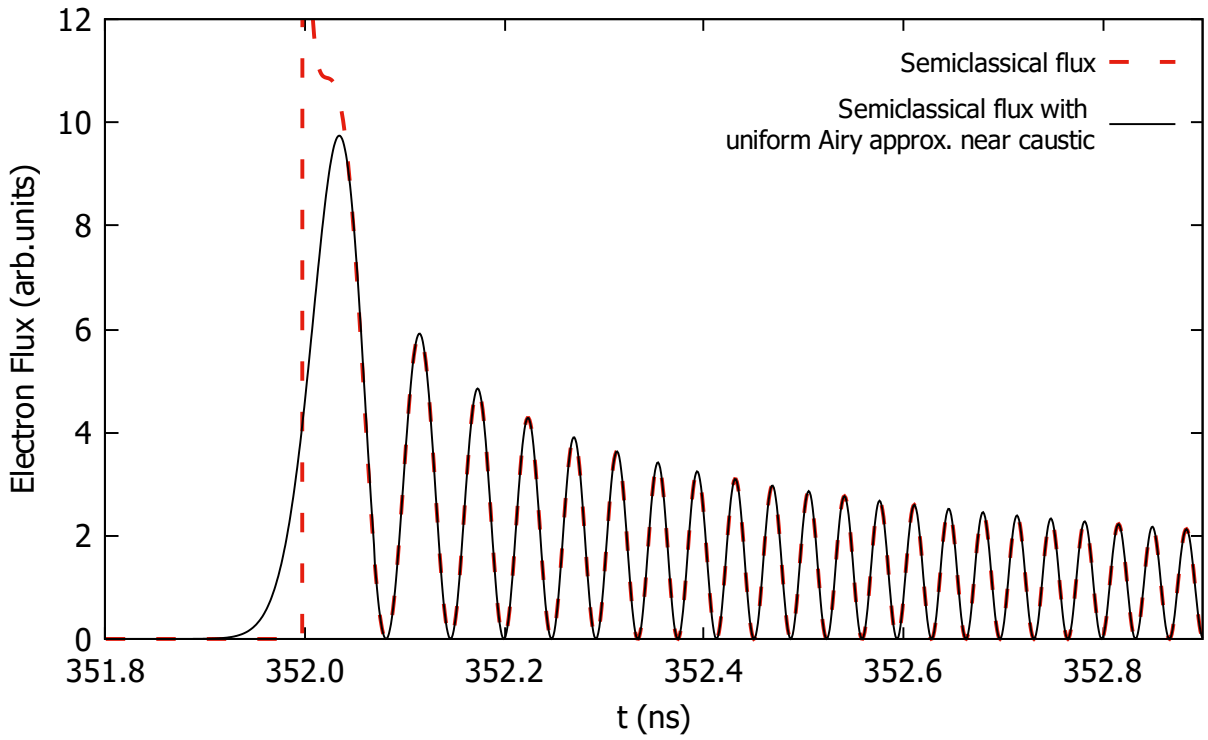

FIG. 6: Electron flux at the center of the detector is shown as a function of time for $F_0 = 50$ V/cm and $\omega = 100$ MHz. Divergence in the semiclassical flux (red dashed line) is corrected using the uniform Airy approximation (thick solid line) near the caustic.

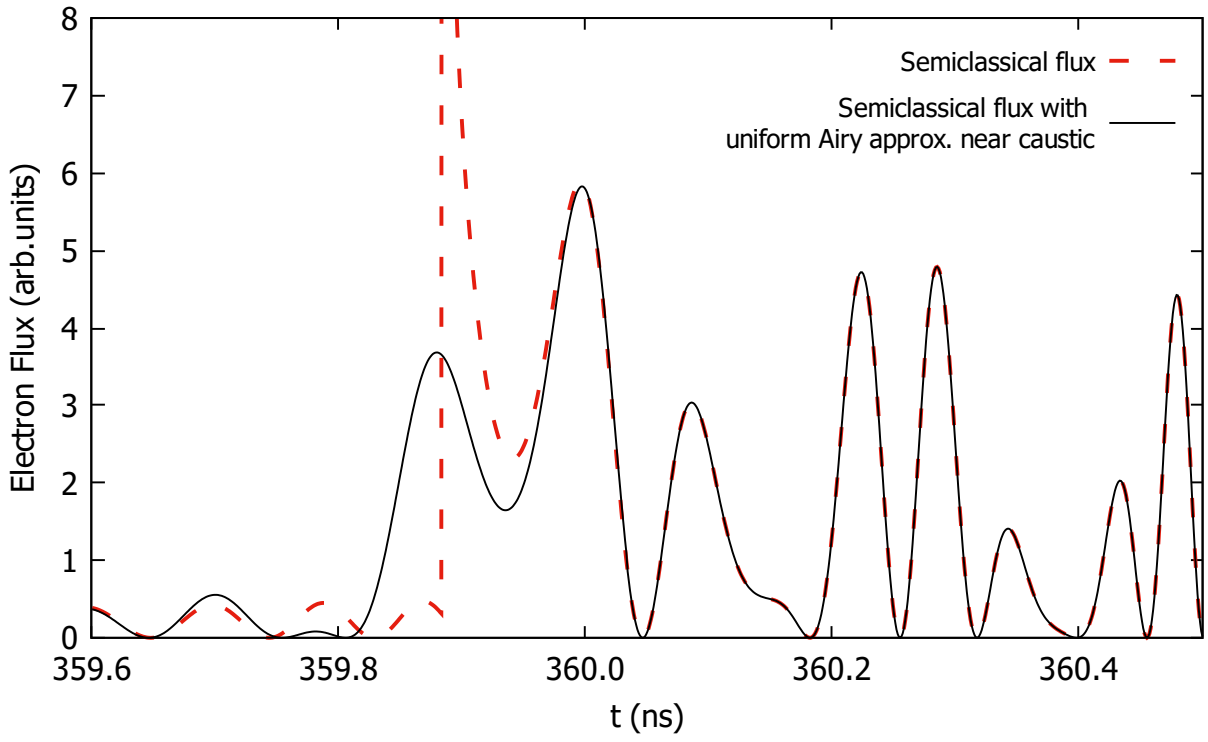

FIG. 7: Same as Fig. 6, but the electron flux near the transition region from 2 to 4 trajectories is shown.

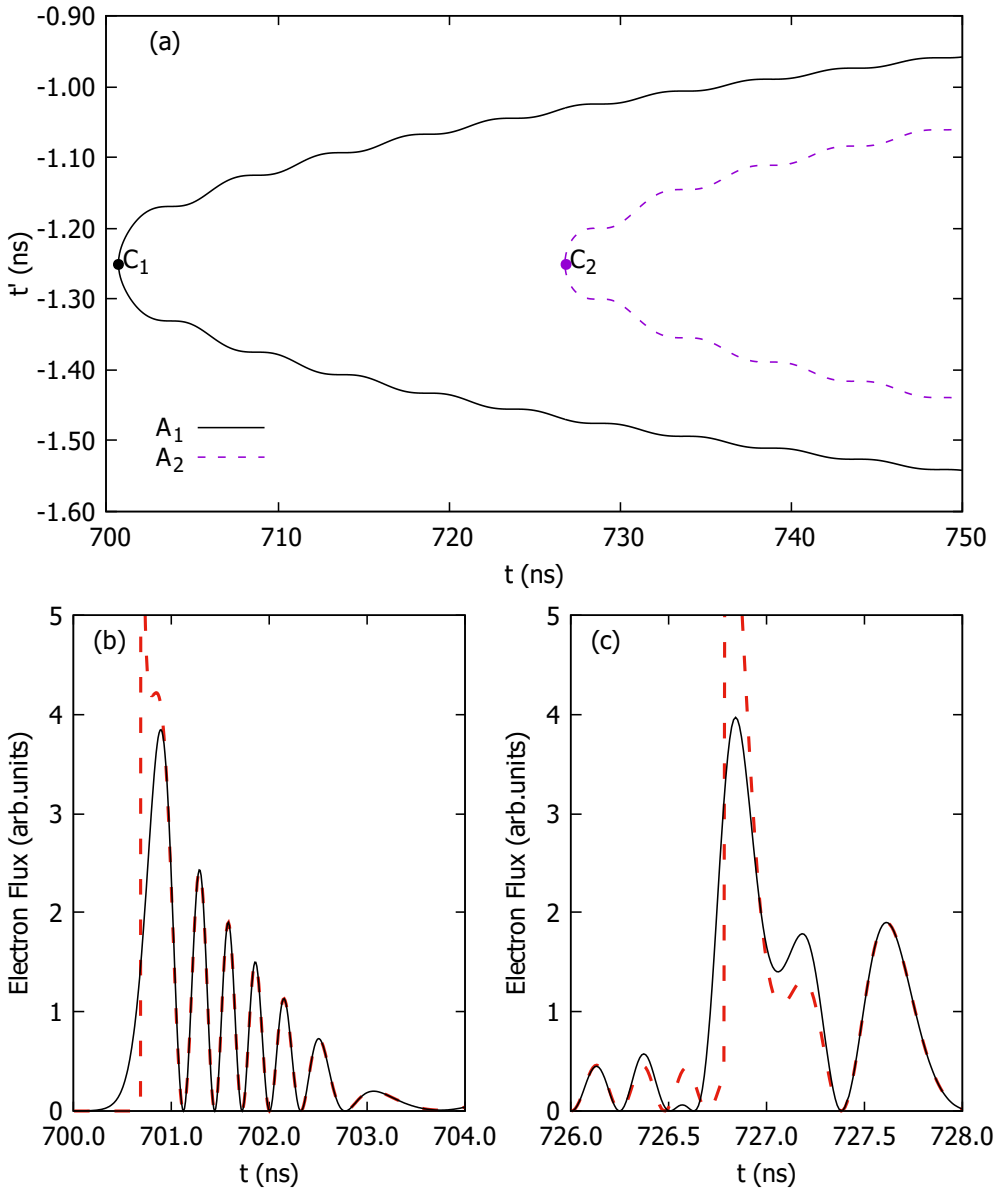

FIG. 8: Calculations for F_0= 50 V/cm and rf 200 MHz. Panel (a): Electron arrival time plot, where C_1 and C_2 indicate the points which satisfy the caustic conditions (16); panel (b): Semiclassical flux (red dashed line) and the uniform Airy function approximation (thick solid line) when the number of electron trajectories increases from 0 to 2. Panel (c): the same as (b), but the number of trajectories increases from 2 to 4

increased to 200 MHz.

It is now interesting to see how the spatial interference pattern changes over the detector plane as the final time t changes. Fig.9 shows that for a fixed final time t, there can be 2 or 4 trajectories arriving at an arbitrary point in the detector. For example, when the final time t=360 ns, there are 4 trajectories arriving at each point in the detector. The interference

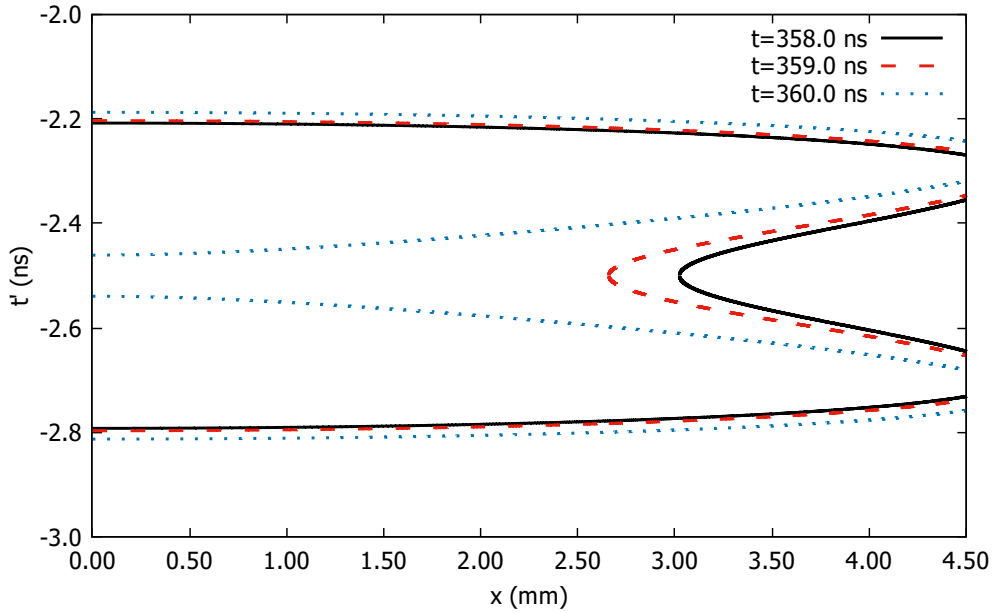

FIG. 9: Initial electron launching time as a function of the x coordinate on the detector plane for different final times t

pattern they produce over the detector plane is shown in Fig. 10. For the final time t=358 ns or t=359 ns, we can again see a transition region from 2 to 4 trajectories along the x coordinate and therefore, a discontinuity in the corresponding semiclassical interference pattern. Similar to the temporal interference pattern, we can remove these divergences using the uniform Airy approximation near the caustics, as shown in Fig. 11. In Fig. 11, we also show the spatial interference pattern of the electrons arriving at the detector plane when the final time t=358 ns and t=359 ns.

VI. CONCLUSION

In conclusion we have investigated photodetachment of negative ions in time dependent low-frequency fields by calculation of the electron flux arriving at a detector which is located at a macroscopic distance away from the photodetachment source. For the calculation of the electron flux, we have used the quantum propagator for the electron motion in a time dependent field and the stationary phase approximation in the evaluation of the wavefunction. Specific calculations were done for H^-, but the approach is easy to extend to multielectron negative ions. We have investigated both temporal and spatial interference structures in the electron flux contributed by two or four electron trajectories. Divergences in the electron flux distribution in both spatial and time domain appear when a new pair of

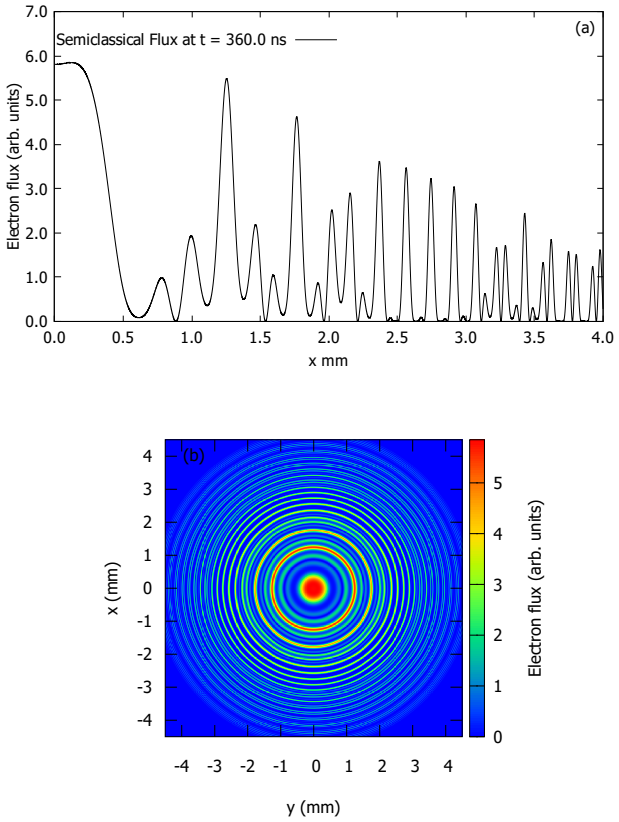

FIG. 10: Panel (a): Variation of the flux along x at t=360 ns (b): Interference pattern in the detector plane. The field amplitude F_0= 50 V/cm and frequency 100MHz,

real electron trajectories emerge from the complex time domain. This pairwise increment of the number of trajectories happens when the point of observation lies on the caustic surface defined by the electron trajectories in space-time domain. The divergences in the electron flux distributions were removed using the uniform Airy approximation near the caustics.

In the current work we did not include the tunneling trajectories. This can be achieved by extending the method we used into complex time domain. For the case of photoioinization in time dependent fields, our method can be modified by inclusion of the long range Coulomb potential into the semiclassical (Van Vleck) propagator [51]. Corresponding classical amplitudes and action are obtained by numerical integration of the classical equations of motion. As a further development of the approach we used here, theory and calculation of the electron flux for a time dependent photoionization microscopy experiment will be presented in a separate paper.

Acknowledgments

This work was supported by the US National Science Foundation of Grants No. PHY-1401788 and EPSCoR RII Track 2.

[1] I. I. Fabrikant, Sov. Phys. JETP **52**, 1045 (1980).

[2] Y. N. Demkov, V. D. Kondratovich, and V. N. Ostrovskii, JETP Lett. **34**, 403 (1981).

[3] M. L. Du, Phys. Rev. A **40**, 4983 (1989).

[4] I. I. Fabrikant, J. Phys. B **23**, 1139 (1990).

[5] M. L. Du, Phys. Rev. A **40**, 1330 (1989).

[6] A. D. Peters, C. Jaffé, and J. B. Delos, Phys. Rev. A **56**, 331 (1997).

[7] Y. Zhao, M. Du, and J.-M. Mao, J. Phys. B **32**, 1409 (1999).

[8] H. J. Zhao and M. L. Du, Phys. Rev. A **79**, 023408 (2009).

[9] B. C. Yang and M. L. Du, J. Phys. B **45**, 175003 (2012).

[10] B. C. Yang, J. B. Delos, and M. L. Du, Phys. Rev. A **88**, 023409 (2013).

[11] B. C. Yang, J. B. Delos, and M. L. Du Phys. Rev. A **89**, 013417 (2014)

[12] C. Blondel, C. Delsart, and F. Dulieu, Phys. Rev. Lett. **77**, 3755 (1996).

[13] C. Blondel, C. Delsart, and F. Goldfarb, J. Phys. B **34**, L281 (2001).

[14] C. Blondel, C. Delsart, C. Valli, S. Yiou, M. R. Godefroid, and S. Van Eck, Phys. Rev. A **64**, 052504 (2001).

[15] C. Blondel, W. Chaibi, C. Delsart, C. Drag, F. Goldfarb, and S. Kröger, Eur. Phys. J. D **33**, 335 (2005).

[16] V. D. Kondratovich and V. N. Ostrovsky, J. Phys. B **23**, 3785 (1990).

[17] C. Nicole, H. L. Offerhaus, M. J. J. Vrakking, F. Lépine, and C. Bordas, Phys. Rev. Lett. **88**, 133001 (2002).

[18] Ch. Bordas, F. Lépine, C. Nicole, and M. J. J. Vrakking, Phys. Rev. A 68, 012709 (2003).

[19] L. B. Zhao and J. B. Delos. Phys. Rev. A **81**, 053417 (2010).

[20] L. B. Zhao and J. B. Delos. Phys. Rev. A **81**, 053418 (2010).

[21] L. B. Zhao, I. I. Fabrikant, J. B. Delos, F. Lépine, S. Cohen, and C. Bordas, Phys. Rev. A **85**, 053421 (2012).

[22] L. B. Zhao, I. I. Fabrikant, M. L. Du, and C. Bordas, Phys. Rev. A **86**, 053413 (2012)

[23] S. Bivona, R. Burlon, and C. Leone, Phys. Rev. A **48**, R3441 (1993).

[24] N. Spellmeyer, D. Kleppner, M. R. Haggerty, V. Kondratovich, J. B. Delos, and J. Gao, Phys. Rev. Lett. **79**, 1650 (1997).

[25] V. Kondratovich and J. B. Delos, Phys. Rev. A **57**, 4604 (1998).

[26] M. R. Haggerty and J. B. Delos, Phys. Rev.A **61**, 053406 (2000).

[27] D.-H. Wang, Z. Chen, and S. Cheng, J. Phys. B **49**, 205001 (2016).

[28] B. C. Yang and F. Robicheaux, Phys. Rev. A **92**, 063410 (2015).

[29] B. C. Yang and F. Robicheaux, Phys. Rev. A **93**, 053413 (2016).

[30] D.-H. Wang, J. Elec. Spectr. Rel. Phenom. **214**, 20 (2017).

[31] D.-H. Wang, Q.-F. Xu, and J. Du, Eur. Phys. J. D **71**, 77 (2017).

[32] W. Becker, F. Grasbon, R. Kopold, D. B. Milošević, G. G. Paulus, and H. Walther, Adv. At. Mol. Opt. Phys. **48**, 65 (2002).

[33] M. Lewenstein, Ph. Balcou, M. Yu. Ivanov, A. L'Huillier, and P. B. Corkum, Phys. Rev. A **49**, 2117 (1994).

[34] V. N. Ostrovsky and J. B. Greenwood, J. Phys. B **38**, 1867 (2005).

[35] G. L. Yudin and M. Yu. Ivanov, Phys. Rev. A **63**, 033404 (2001).

[36] P. B. Corkum, Phys. Rev. Lett. **71**, 1994 (1993).

[37] J. B. Delos and M.-L. Du, IEEE J. Quant. Electronics **24**, 1445 (1988).

[38] W. H. Miller, Adv. Chem. Phys. **25**, 69 (1974); **30**, 77 (1975).

[39] J.-M. Mao, J. Shaw and J. B. Delos, J. Stat. Phys. **68**, 51 (1992).

[40] A. M. Perelomov, V. S. Popov, and A. M. Terent'ev, Sov. Phys. JETP **24**, 207 (1966).

[41] W. H. Miller and T. F. George, J. Chem. Phys. **56**, 5668 (1972).

[42] V. S. Popov, Yad. Fiz. **68**, 717 (2005) [Phys. At. Nucl. **68**, 686 (2005)].

[43] I. I. Fabrikant and G. A. Gallup, Phys. Rev. A **79**, 013406 (2009).

[44] D. B. Milošević, G. G. Paulus, D. Bauer, and W. Becker, J. Phys. B **39**, R203 (2006).

[45] T.-M. Yan, S. V. Popruzhenko, M. J. J. Vrakking, and D. Bauer, Phys. Rev. Lett. **105**, 253002 (2010).

[46] R. P. Feynman, Rev. Mod. Phys. **20**, 367 (1948); R. P. Feynman and A. R. Hibbs, *Quantum Mechanics and Path Integrals*. New York, McGraw-Hill, 1965.

[47] I. I. Fabrikant, J. Phys. B **27**, 4545 (1994).

[48] I. I. Fabrikant, Phys. Rev. A **66**, 010703 (2002).

[49] N. L. Manakov, M. V. Frolov, A. F. Starace, and I. I. Fabrikant, J. Phys. B **33**, R141 (2000).

[50] M. L. Du and J. B. Delos, Phys. Rev. A **38**, 5609 (1988).

[51] M. C. Gutzwiller, J. Math. Phys. **8**, 1979 (1967).

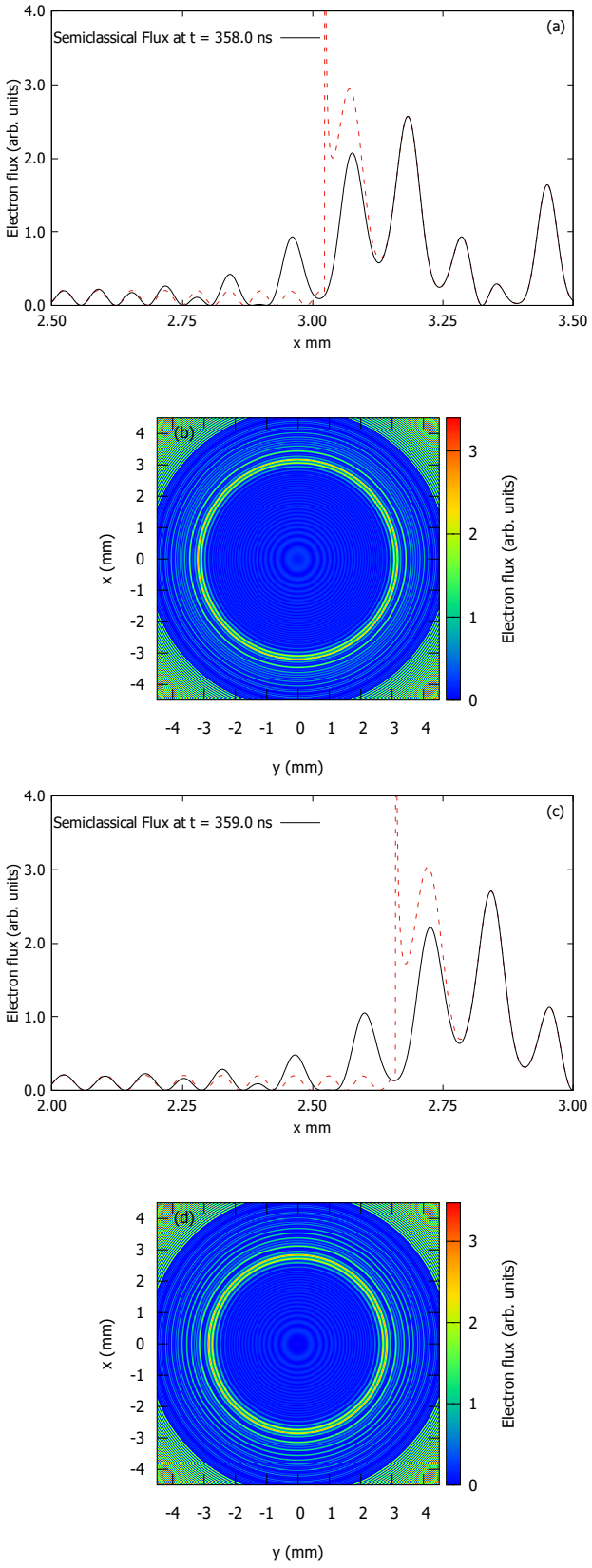

FIG. 11: Panels (a) and (c) show the variation of the spatial interference pattern along the x coordinate for t= 358 ns and t=359 ns, respectively. Panels (b) and (d) show the corresponding spatial distribution of the electron flux in the detector plane.